ACS OMEGA

http://pubs.acs.org/journal/acsodf

Article

Effects of Surface Roughness on Direct Plasma Bonding between Silicone Rubbers Fabricated with 3D-Printed Molds

Yujin Jang,* Hiroyuki Nabae, and Koichi Suzumori

Cite This: *ACS Omega* 2022, 7, 45004−45013

Read Online

ACCESS | Metrics & More | Article Recommendations

ABSTRACT: This study presents the effects of surface roughness on the adhesion strength of plasma-treated rubbers that are widely used in soft robotics. The rubbers are designed with 11 molds of different patterns and fabricated from liquid silicones for mutual comparison. Several specimens with nonperiodic and periodic surface waveforms are quantitatively analyzed based on the correlation between surface roughness and adhesion strength. The surface roughness of three-dimensional (3D) printed molds under different printing conditions is compared to that of the standard specimens molded by a smooth acrylic plate and four sandpapers. The surface profiles are measured by a stylus profiler, analyzed using fast Fourier transform, and subsequently quantified using the experimental roughness parameters, R_a and R^*_{ku}. The kurtosis ratio R^*_{ku} is proposed to simultaneously evaluate the sharpness, total height, and peak density to identify contact surfaces. A 90° peel test is also conducted to evaluate the adhesion strength, considering the designed pattern and printing orientation relative to the peeling direction. Microstructural analysis of the specimens is performed to investigate the peeling mechanism and molding quality using scanning electron and digital microscopes. Correlations between adhesion strength and surface roughness are obtained through the evaluation of the plasma-treated silicone specimens. R^*_{ku} is significant in determining the surface properties of the effective contact area, particularly for rough surfaces, and further contributes to an effective evaluation when the parameter R_a is used simultaneously. The results suggest that the plasma bonding of silicone rubbers fabricated with 3D-printed molds is effective in enhancing the adhesion strength of soft robots or stretchable devices.

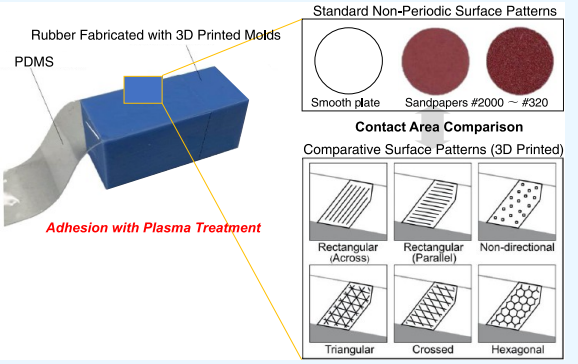

1. INTRODUCTION

Multifunctional systems based on biological mechanisms are attracting attention because of their inherently soft and elastically deformable movements.[1−3] A soft robot has a main body and moving parts consisting of elastic materials, such as polymers, gels, silicone, and other flexible materials. Soft robots are fabricated using shape deposition manufacturing (SDM),[4,5] three-dimensional (3D) printing technology,[6,7] and smart composite microstructure (SCM).[8,9] However, the current fabrication methods are challenging.

Among these methods, SDM, commonly called molding, using liquid rubbers has been widely introduced to develop soft robots.[10] It can quickly produce various soft materials with the desired shapes and sizes and no postprocessing is required in the molding process. With higher design freedom and the possibility of simultaneous surface structures, custom-designed molds can develop customized prototypes and realize the desired movements in soft robotics.[11,12]

With 3D printing technology, even complex molds can be easily printed with a 3D printer, and molded rubber can be shaped into any desired structure. The molds are printed directly using computer-aided design (CAD) files, thereby realizing an efficient process for designing, fabricating, and implementing their respective soft robotic systems. The aforementioned advantages have been exploited by casting prototypes on 3D-printed molds for the fabrication of flexible soft robots, including linear actuators,[13] tactile sensors,[14] robot arms,[15] microfingers,[16] and grippers.[17] Zhang et al. successfully fabricated a patterned mold-based prototype with high flatness and flexibility; this is an interesting work related to the formation of microstructured molds using a 3D printer.[18] Despite its cost-effective and fast prototyping, limitations in terms of precision and surface finish have been reported.

Liquid silicone rubber is considered an important material for soft robots owing to its excellent chemical/thermal stability, low toxicity, flexible movements, and ease of integration into the structure. Moreover, because silicone provides high tensile strength and elasticity, these soft robots can be easily extracted

Received: August 18, 2022
Accepted: November 14, 2022
Published: November 30, 2022

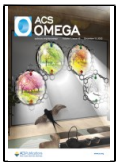

from 3D-printed molds. The properties of silicones are well-suited for creating stretchable sensor skins,[19,20] microfluidic channels,[21] and pneumatic cavities for entirely soft robotics.[13,22] For example, a snake-inspired soft robot employed silicone rubbers with multiple internal chambers to achieve serpentine locomotion.[23] An octopus-inspired robot used a silicone arm with embedded cables to deform the segment in the desired manner and replicate the functionality of the muscular structure of the octopus arm.[24] The structure of this system can directly mimic that of the muscle system and engage in biomimetics.

The enhancement of bonding technology through the advanced processing of soft materials is also closely related to the development of soft devices. Research is being conducted on methods for rubber bonding, such as plasma,[13] arc,[25] UV light,[26] and laser treatments.[27,28] Research on bonding technology based on rubbers and processing treatments has been reported. Yamamoto experimentally demonstrated that atmospheric plasma is a promising technique for realizing surface modification from hydrophobic to hydrophilic and bonding of silicone elastomers.[29] Gaboury et al. developed microwave plasma treatments to chemically bond the solid monomers on silicone and functionalized surfaces.[30] Moreover, adhesion with low variation can be achieved by uniform modification.[31]

For 3D-printed mold-based rubbers, the rubber surface and its roughness are determined by the surface waveforms of the 3D-printed mold. In 3D printing, layers of molten thermoplastics are deposited successively according to the design. The layer width and height have a significant influence on the waveforms, resulting in different contact areas. A previous study demonstrated that surface roughness is influenced by printing speed,[32] printing orientation,[33] layer height,[34−36] and layering structure.[37]

Several studies have investigated the correlation between the adhesion strength and roughness parameters, such as the arithmetic mean deviation R_a[38,39] and kurtosis R_{ku}.[40−42] R_a provides a good overall description of height variations; however, it does not describe any information on wavelengths and therefore is not sensitive to contact surfaces for small changes. Meanwhile, R_{ku} describes the flatness or peakedness of the peaks; however, it does not give a detailed description of the contact surface. The Pearson system[43] has demonstrated that the density of the asperity distributions results in adhesion. Because the roughness of the contact surface can be modeled by a number of peaks with different kurtosis values, the kurtosis ratio R^*_{ku} is proposed in the present study.

In addition, the effects of surface roughness on the adhesion strength of plasma-treated rubbers used in soft robots have been investigated. Surface roughness is considered an important parameter in determining the adhesion performance of the bonded interface. Quantitative test measurements are performed on silicone/silicone composites to increase adhesion and maintain flexibility. Thin membranes are bonded to various silicone substrates fabricated using 3D-printed molds. The surface of the silicone substrate is studied by fast Fourier transform (FFT), characterized by both the average roughness and newly presented parameters, and investigated by microstructural analysis. Based on the experimental results, the adhesive properties of plasma-treated silicone rubber are quantitatively compared and analyzed under various conditions.

2. MATERIALS AND METHOD

2.1. Specimen. The specimen used for the peel test consisted of a silicone membrane mounted on flexible rubber,

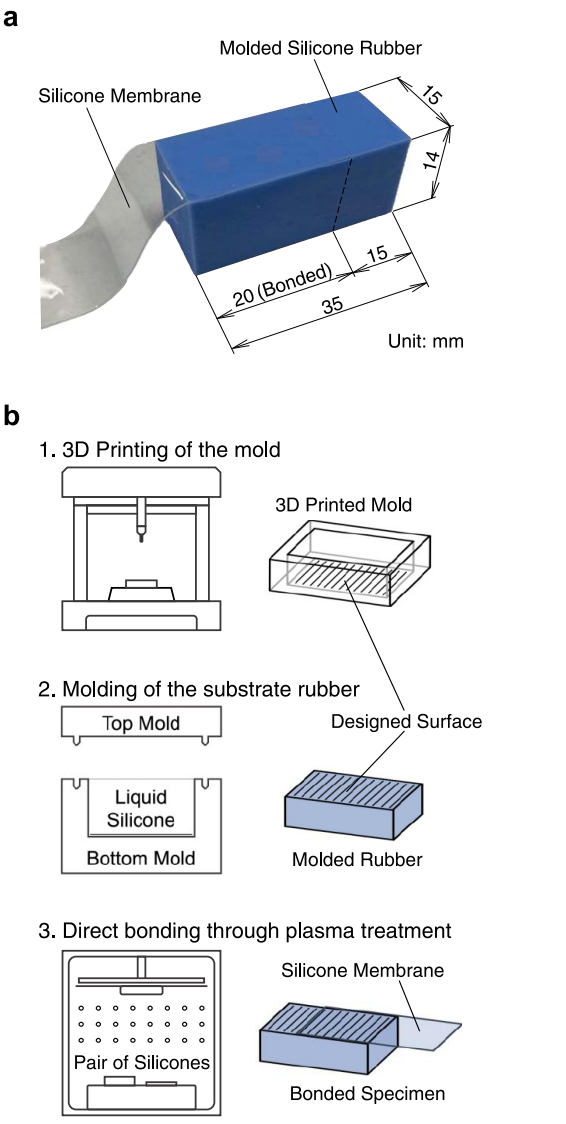

Figure 1. Peel test specimen. (a) Fabricated specimen. (b) Schematic illustrations of the fabrication process.

Table 1. Surface Symbols for Standard and Comparative Samples

type of surface	symbol
acrylic plate	S1
P2500-grit sandpaper	S2
P1200-grit sandpaper	S3
P1000-grit sandpaper	S4
P320-grit sandpaper	S5
Objet260 rectangular across	P1
Objet260 rectangular parallel	P2
mark two triangular	P3
mark two hexagonal	P4
M200 PATT.0 crossed	P5
M200 PATT.2 hexagonal	P6

https://doi.org/10.1021/acsomega.2c05308
ACS Omega 2022, 7, 45004−45013

Table 2. Conditions for the Mold Fabrication Using 3D Printers

3D printer (manufacturer)	prototyping method	layer thickness, μm	material	fill pattern	printing orientation
Objet260 Connex (Stratasys)	Polyjet	30	Vero White	rectangular	across
mark two (Markforged)	FDM	100	Onyx	triangular hexagonal	parallel
M200 (Zortrax)	FDM	290	Z-ULTRAT	crossed hexagonal	

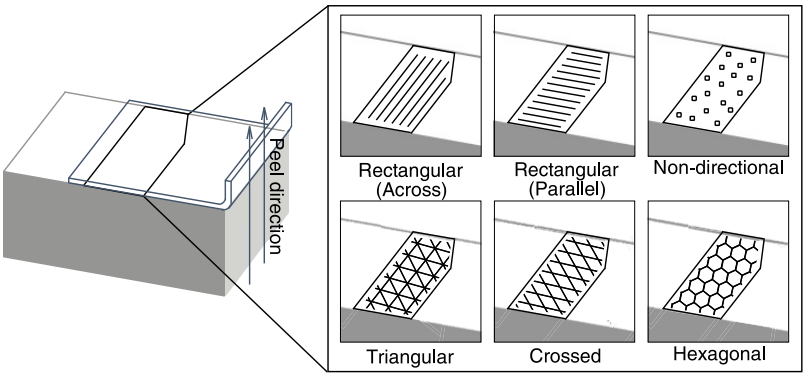

Figure 2. Fill patterns designed to assess surface roughness.

Figure 3. Photograph of the 90° peel test.

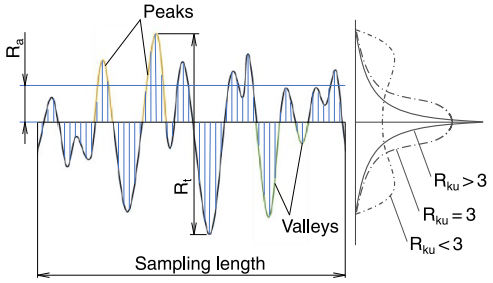

Figure 5. Roughness profile indicating R_a, R_t, and R_{ku}.

which was molded using 3D-printed components, as shown in Figure 1a. Figure 1b shows the fabrication process in three main steps: (a) 3D printing of the mold, (b) molding of the substrate rubber, and (c) direct bonding through atmospheric plasma treatment. A high-precision silicone membrane with a thickness of 200 μm (ELASTOSIL Film 2030, Wacker Chemie AG) was used. The 3D-printed molds were specified to produce silicone rubbers with a length, width, and height of 35, 15, and 14 mm, respectively. The membranes were mounted on the molded silicone rubbers of length 20 mm, as shown in Figure 1a. Molded rubber is a commercial product of liquid silicone (KE/CAT−1600, Shin-Etsu Silicones Corp.), which is

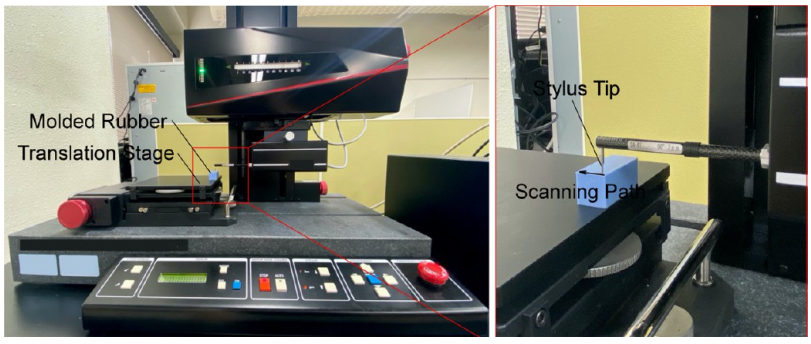

Figure 4. Stylus surface profiler used for measuring surface roughness.

https://doi.org/10.1021/acsomega.2c05308
ACS Omega 2022, 7, 45004−45013

Table 3. Surface Roughness Parameter R_a for 11 Samples

	roughness parameter R_a, μm						
type of surface	test 1	test 2	test 3	test 4	test 5	average	standard deviation
S1	0.336	0.227	0.330	0.342	0.317	0.310	0.043
S2	2.730	2.668	3.368	3.122	3.454	3.068	0.321
S3	4.856	5.190	4.376	5.588	5.485	5.099	0.442
S4	5.206	5.654	7.626	5.385	6.759	6.126	0.924
S5	13.314	9.302	12.065	10.118	12.151	11.390	1.464
P1	0.775	0.928	0.433	0.494	0.865	0.699	0.199
P2	1.564	1.673	1.847	2.252	1.576	1.782	0.355
P3	4.400	4.459	3.810	3.388	3.983	4.008	0.395
P4	4.535	4.794	4.463	5.461	4.570	4.765	0.365
P5	6.458	7.577	7.001	7.009	7.070	7.023	0.355
P6	9.040	9.151	9.384	8.484	8.137	8.839	0.459

Table 4. Surface Roughness Parameter R^*_{ku} for 11 Samples

	roughness parameter R^*_{ku}, μm^{-1}						
type of surface	test 1	test 2	test 3	test 4	test 5	average	standard deviation
S1	18.225	18.974	20.143	17.087	17.975	18.481	1.027
S2	5.678	5.893	7.087	6.945	6.389	6.398	0.557
S3	2.741	2.850	2.544	3.369	3.143	2.929	0.293
S4	1.518	1.930	2.451	1.501	2.071	1.894	0.357
S5	0.559	0.296	0.526	0.686	1.099	0.627	0.273
P1	15.584	11.360	11.911	10.720	11.376	12.190	1.738
P2	8.964	10.087	7.073	8.3053	9.459	8.778	1.034
P3	3.899	4.542	5.245	4.022	4.589	4.460	0.479
P4	3.605	3.843	3.343	3.290	4.127	3.642	0.313
P5	1.775	1.283	1.027	1.399	0.846	1.266	0.320
P6	1.250	0.567	0.637	0.808	0.843	0.821	0.238

widely used in soft robotics. Here, curing was conducted at a room temperature of 18 °C to keep the hardness of the substrate specimen constant.

Eleven different types of surface roughness were introduced, as listed in Table 1. First, five standard specimens were quantitatively analyzed to determine the correlation between surface roughness and adhesion strength. The specimens were smooth acrylic plate, P2500-grit sandpaper, P1200-grit sandpaper, P1000-grit sandpaper, and P320-grit sandpaper. The other six specimens were designed and fabricated using three 3D printers: Stratasys Objet260 Connex3, Markforged Mark Two, and Zortrax M200 printer. The surface types determined by standard specimens are denoted by "S" and those by 3D-printed molds as "P". The standard specimens with non-periodic waveforms are denoted S1−S5, while the comparative specimens with periodic waveforms are denoted P1−P6.

The main factors influencing the adhesion strength are fill pattern, material, layer thickness, and printing orientation relative to the peel direction. The printing parameters are listed in Table 2. The evaluation results indicate that the quality of the molded surface is not affected by the support material because the material is not located on its surface, as shown in Figure 1b. The fill patterns displayed on the molded rubbers are illustrated in Figure 2. To evaluate the effects of surface roughness on the adhesion strength between rubbers, six fill patterns were introduced: rectangular (across), rectangular (parallel), nondirectional, triangular, crossed, and hexagonal.

The plasma treatment equipment (CIONE, Femto Science Inc.) was utilized for direct bonding. While maintaining the air flow rate at 10 sccm (standard cubic centimeter per minute), plasma was obtained at a predetermined pressure of 7.6×10^2 Torr with a radio frequency (RF) power of 100 W. The base pressure was maintained at less than 5.0×10^{-2} Torr, and the plasma exposure time was set to 30 s to minimize variations in surface energy for all specimens.

2.2. Measurement of Adhesion Strength. A 90° peel test was performed to evaluate the stress/strain relationships when the plasma-treated rubbers were subjected to a uniaxial tensile load. Figure 3 shows the experimental apparatus of the peel test using a tensile tester (EZ−LX, Shimadzu Inc.) equipped with a 500 N load cell. It should be noted that the molded silicone rubber has a hardness shore A value of 45, which is a sufficiently large value compared to that of the membrane (hardness shore A value of 27). The end of the unbonded portion of the membrane was lifted with a velocity of 6 mm/min at a room temperature of 18 °C. To determine the adhesion strength, the average of three measurement iterations was used for each condition.

2.3. Measurement of Surface Roughness. The surface roughness of all rubber substrates in the width direction was measured using a stylus surface profiler (DSF600, Ryokosha Co.) with a stylus tip radius of 2 μm, as shown in Figure 4. The black arrow indicates the scanning path. According to the measurement condition of ISO 4288, the stylus travel and measurement speed are 15 mm and 0.05 mm/s, respectively. The profiler had a vertical resolution of 12 nm and a vertical measuring range of 8 mm.

The FFT provided by MATLAB software was introduced to perform frequency analysis using the variation in roughness profiles. First, it eliminates the displacement that occurs when the specimen is not parallel to the translation stage, or the presence of geometric defects, such as scratches, dents, and

https://doi.org/10.1021/acsomega.2c05308
ACS Omega 2022, 7, 45004−45013

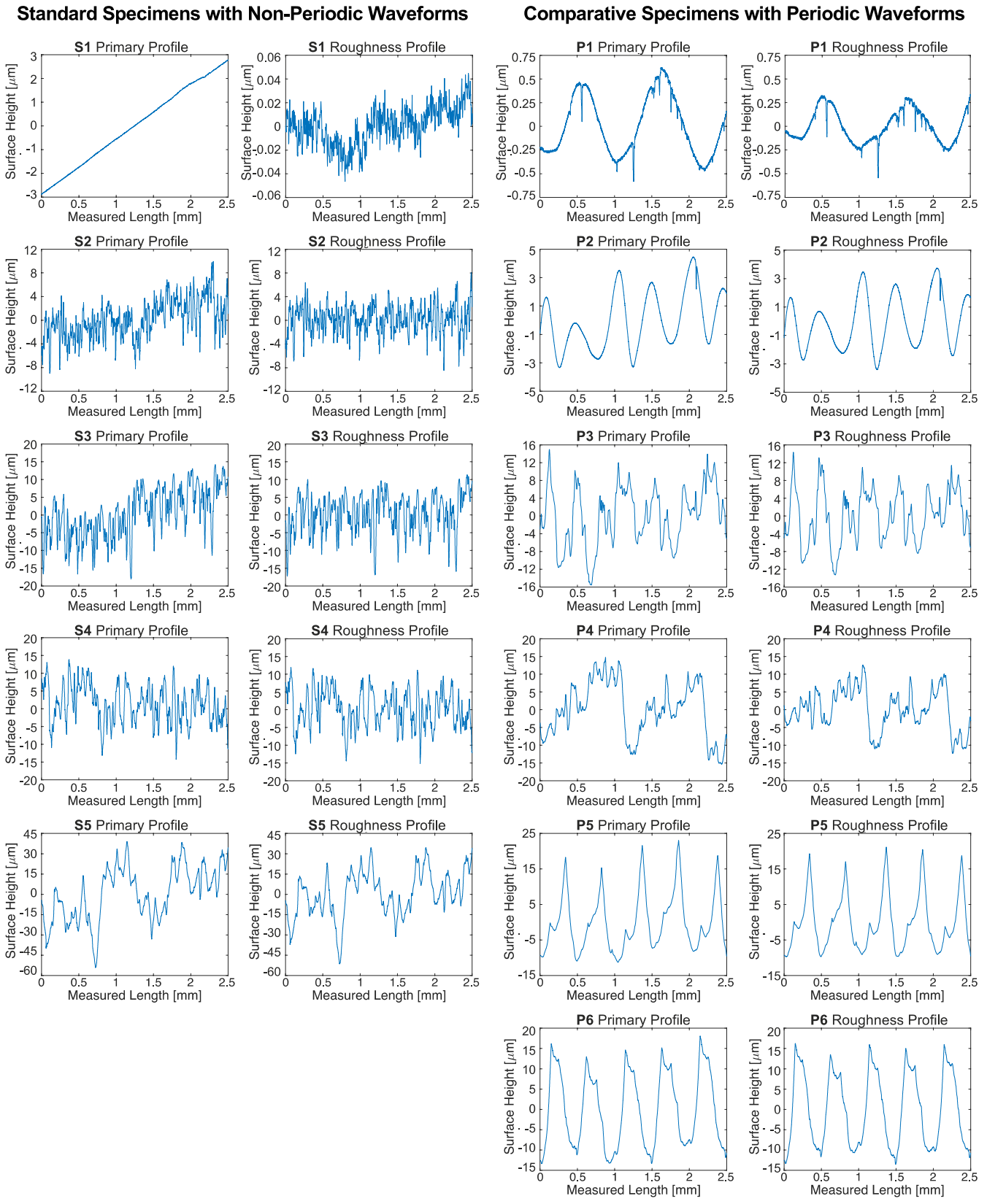

Figure 6. Primary and roughness profiles obtained through FFT for all specimens.

cracks. After filtering out the high-frequency signal, the separated spectra were computed to obtain the experimental surface roughness parameters using the inverse FFT (IFFT). Based on the obtained phase distribution, R_a and R_{ku}^* are calculated.

The roughness parameter R_a provides a good overall description of height variations. However, it does not describe

https://doi.org/10.1021/acsomega.2c05308
ACS Omega 2022, 7, 45004−45013

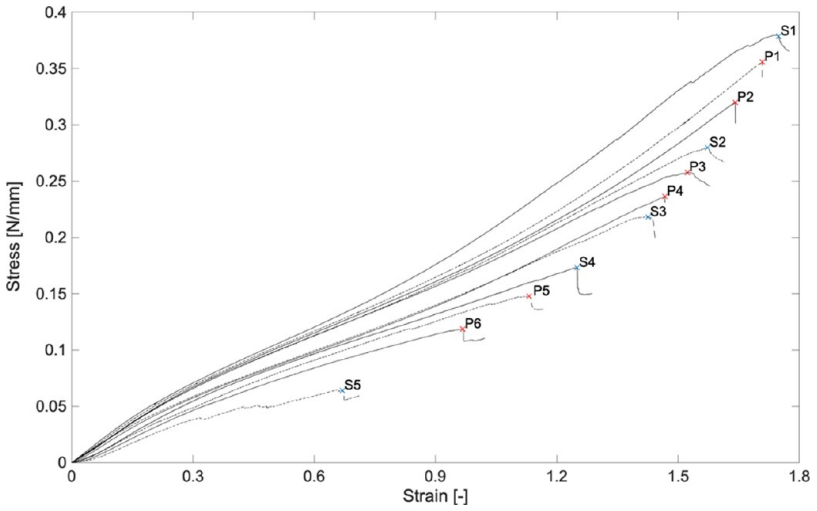

Figure 7. Stress−strain curves for 11 types of surface properties.

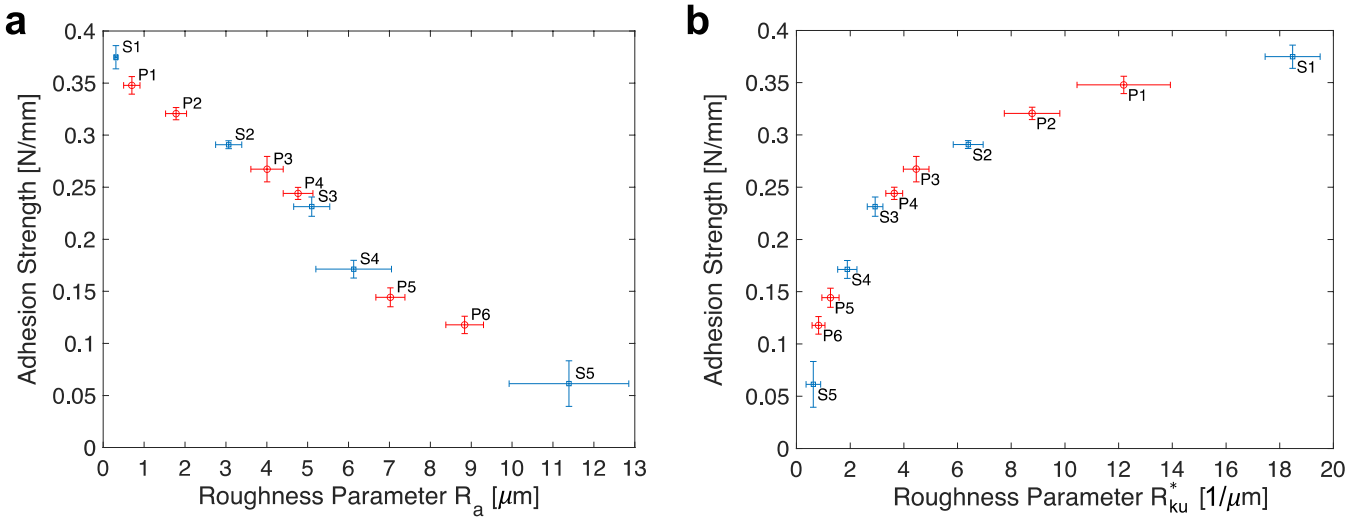

Figure 8. Adhesion strength with respect to roughness parameters (a) R_a and (b) R^*_{ku}.

the contact surface clearly; therefore, different surfaces can have a similar R_a value and vice versa. It also does not provide any information on wavelengths and reacts sensitively to small deviations in the profile.

Moreover, kurtosis is important for describing the effective contact area that affects the direct bonding performance at the interface between rubbers. The standard kurtosis parameter R_{ku} represents the probability density sharpness of the profile. Therefore, it is suitable for analyzing the degree of contact between two objects. For surfaces with a sharp height distribution, R_{ku} is less than 3, whereas that for surfaces with a flattened height distribution is greater than 3. When the rubbers were bonded together, the area of the interface included the peaks and the area around them. Thus, the bonding performance is dependent not only on kurtosis but also on the peak-to-valley height and peak density. In the present study, the experimental parameter R^*_{ku} was introduced to simultaneously evaluate the sharpness of the profile, total height, and peak density. The proposed kurtosis ratio R^*_{ku} is defined as follows

$$R^*_{ku} = \frac{R_{ku} RP_c}{R_t}$$

where R_{ku} is the kurtosis, RP_c is the peak count number, and R_t is the height between the highest peak and lowest valley in the evaluation length. Figure 5 provides a schematic illustration of the parameters R_a, R_t, and R_{ku} for the roughness profile.

The detailed surface characteristics were inspected using a scanning electron microscope (SEM, VE8800, Keyence) and a digital microscope (VHX−7100, Keyence). The molded, exfoliated, and fractured surfaces of the specimens were then investigated. The specimens were osmium sputtered prior to SEM observations using an osmium coater (Neoc−Pro, Meiwafosis Co.).

3. RESULTS AND DISCUSSION

3.1. Evaluation of Roughness Parameters. Surface measurements were performed to evaluate the roughness parameters of the silicone rubbers fabricated using standard and comparative molds. Roughness profiles were obtained by primary profiles with a sampling length of 2.5 mm through FFT and IFFT. A filter with a 0.4 mm^{-1} cutoff wavelength was

https://doi.org/10.1021/acsomega.2c05308
ACS Omega 2022, 7, 45004−45013

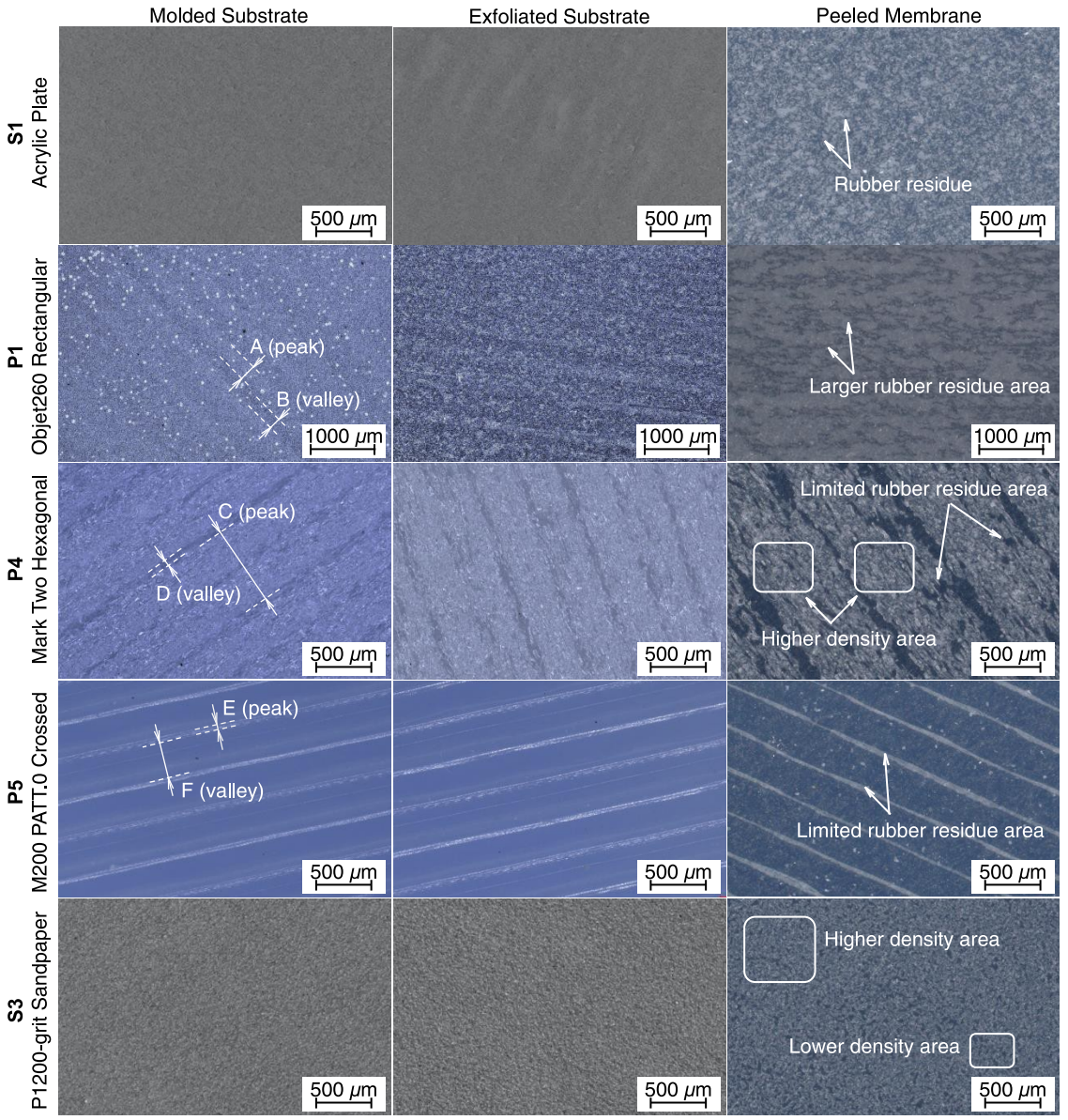

Figure 9. Microstructural images: molded substates, exfoliated substates, and peeled membranes.

used. The average roughness parameters R_a and R^*_{ku}, which are determined by five iterative measurements, are shown in Tables 3 and 4, respectively. Figure 6 shows the primary and roughness profiles of all specimens under the designated spatial frequency. While the surfaces of specimens S1−S5 show nondirectional and nonperiodic patterns, those of specimens P1−P6 have periodic waveforms.

3.2. Silicone Rubber/Rubber Adhesion. The rubbers were designed and molded on the surface of the 11 specimens to evaluate the effects of surface roughness on the peel-off strength. The minimum force required to separate the thin membrane from the substrate was defined by the adhesion strength. Figure 7 shows the stress−strain curves of the standard and comparative specimens. To determine the adhesion strength, the stress was determined by averaging three or more measurements. As shown in Figure 7, rubber S1 has the highest tensile stress, whereas, rubber S5 has the lowest value. The stress increases linearly with strain until the specimen was separated. It is observed that the specimen with a higher peel strength separated at a higher strain.

To analyze the effect of surface roughness on the direct bonding performance, the experimental roughness parameters R_a and R^*_{ku} were obtained from the transformed roughness profiles. Figure 8a shows a comparison of the adhesion strength with respect to R_a. Based on the analyzed data of standard specimens S1−S5, the adhesion strength decreased almost linearly with R_a. The comparative specimens P1−P6 with periodic waveforms are observed to be consistent, and surfaces with a higher average height distribution tend to deteriorate the direct bonding performance. The rubber P1 provided strong adhesion and a smooth surface finish, similar to rubber S1. The printing orientation relative to the peel direction significantly influenced the bonding performance as inferred from the comparison between rubbers P1 and P2. However, rougher specimens show greater variability for nondirectional and nonperiodic surfaces. Thus, R_a is not sufficient to determine the effect on contact surfaces for these features. However, R_a is important in evaluating smooth surfaces.

https://doi.org/10.1021/acsomega.2c05308
ACS Omega 2022, 7, 45004−45013

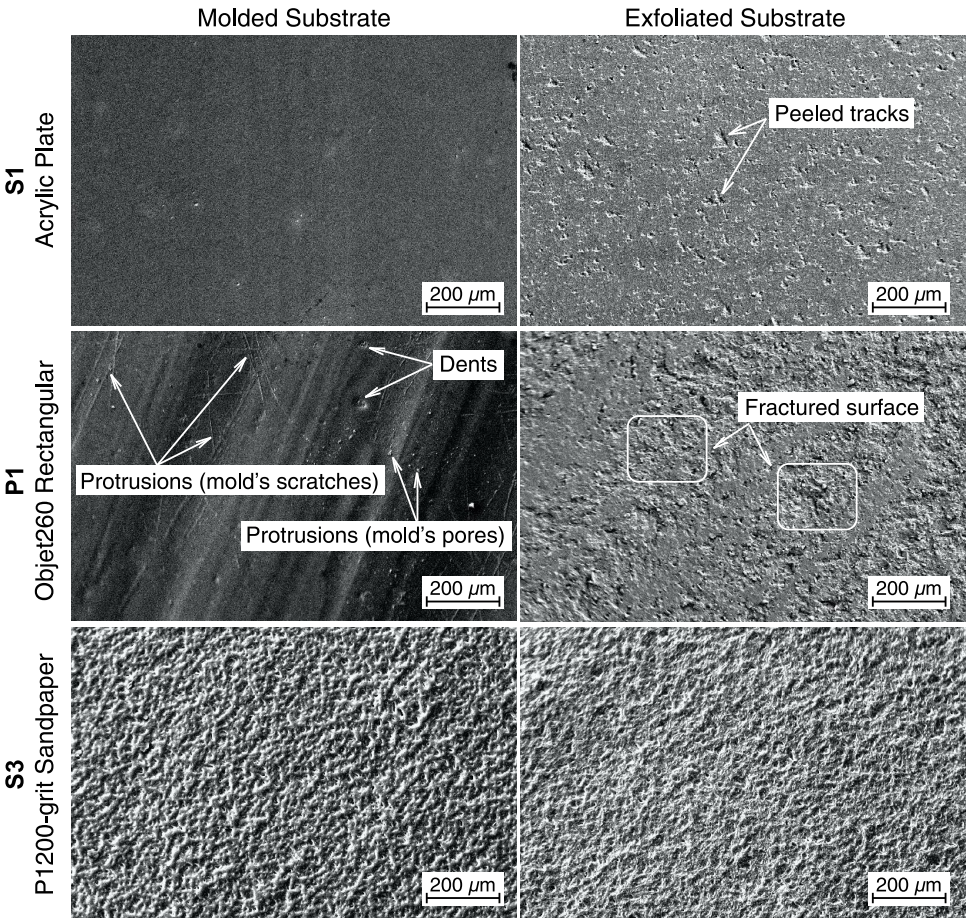

Figure 10. SEM images for molded and exfoliated substrates.

Figure 8b shows the adhesion strength with respect to R_{ku}^{*}. For each specimen, the contact conditions were different. Therefore, kurtosis was evaluated according to the total height and peak density simultaneously. The correlation between R_{ku}^{*} and adhesion strength was clearly obtained, and the rubbers S1−S5 and P1−P6 were observed to be consistent. The results showed that the fill pattern and printing orientation relative to the peel direction on the molded surfaces affected the adhesion performance. Rubber S1 had a relatively flat height distribution, low peak-to-valley height, and high peak density, thus resulting in the strongest adhesion strength. However, rubber P6 had the flattest height distribution, but a high peak-to-valley height and low peak density, thus resulting in low adhesion strength. Therefore, R_{ku}^{*} is confirmed to be useful in analyzing specimens with different peaks and valleys. However, smooth specimens exhibited relatively large variability for R_{ku}^{*}, while R_a in these cases showed low variability. Because the parameter R_a is not sensitive to low-height peaks, the variation value is low, particularly for a smooth surface. However, R_{ku}^{*} is experimentally verified to respond sensitively on a smooth surface because it considers the distance between the peaks and valleys, thus resulting in a relatively large variation value. Moreover, it can discriminate between rough surfaces, thus achieving effective evaluation when the two parameters are used simultaneously.

3.3. Microstructural Observations of Specimen Surfaces. A digital optical microscope and SEM were used to identify the features of the molded, exfoliated, and peeled surfaces of the specimens. Figure 9 shows the microstructural images of the molded rubber, exfoliated rubber, and peeled membrane under five representative conditions: acrylic plate (S1), Objet260 rectangular (P1), Mark Two hexagonal (P4), M200 PATT.2 crossed (P5), and P1200-grit sandpaper (S3).

The standard specimens S1 and S3 had nondirectional and nonperiodic pattern features. The comparative specimens P1, P4, and P5 exhibited periodic waveforms. As shown in Figure 9, they demonstrate a straight printing orientation and a consistent distance between the wave peaks and valleys, thus confirming regular surface formation. These regular surface morphologies were negative for the surface conditions of the 3D-printed molds. The peak and valley widths were approximately 256.6 and 193.9 μm, corresponding to A and B scanning paths, respectively. For P4, the peak and valley widths were approximately 734.8 and 54.0 μm, corresponding to C and D scanning paths, respectively. Moreover, for P5, the peak and valley widths were approximately 50.3 and 327.0 μm, corresponding to E and F scanning paths, respectively, thus resulting in the weakest adhesion. Although P4 had a wider peak width, P1 exhibited a stronger bonding performance because it had short and gentle curves in the vertical plane, which can be confirmed from the images of the peeled membrane. In this case, no distinct regularity appeared on the peeled membrane, indicating that the height between the deepest valley and the highest peak was low. This was consistent with the surface measurement results as shown in Figure 6. It should be noted that not only the peak width but also the depth difference in the waveforms contributed to the bonding performance.

https://doi.org/10.1021/acsomega.2c05308
ACS Omega 2022, 7, 45004−45013

From the peeled membrane images, the rubber residues that were detached from the substrates can be observed on their membranes. The adhesive bonding area was distributed along the rubber protrusion patterns, that is, on the peaks and the area around them. This indicated that the bonding characteristics of the plasma-treated specimens were significantly affected by the surface patterns of the molded rubbers.

To observe the detailed features between the molded and exfoliated rubber surfaces, additional SEM images were captured for S1, P1, and S3, as shown in Figure 10. The surface of the initially molded substrates indicates molding quality. Defects, such as small pores and scratches on the 3D-printed molds, are formed on the substrate. Moreover, some dents that were generated during the molding process, emerged on the surface. Complex holes of various sizes and depths were formed on the exfoliated surfaces after the 90° peel tests. While the exfoliated substrate S1 had scattered and detached tracks, the fractures on P1 were dominant in the wave peaks and the area around them.

4. CONCLUSIONS

The surface roughness and its influence on the adhesion strength between silicone rubbers fabricated by 3D-printed molds have been investigated. The rubbers were designed with 11 molds of different patterns, directly bonded by plasma treatment, and then compared to evaluate the effectiveness of their assembly to manufacture a soft robot. Surface measurements and 90° peel tests were performed to verify the effect of surface roughness on the adhesion strength between rubbers. The surface properties of the rubber substrates determined by the 3D-printed molds were evaluated, and the features were quantitatively analyzed using R_a and R^*_{ku}. The results are summarized as follows.

The molded rubber surface is closely related to the adhesion strength of silicone composites. The effect of the surface roughness features is observed using nondirectional surfaces, such as an acrylic plate and sandpapers as standard specimens. The experimental parameters, R_a and R^*_{ku}, show good correlations. R_a is not sufficient to determine the surface roughness of rough and nonperiodic specimens. R^*_{ku} is determined by the total height and peak density simultaneously; thus, it is validated to represent the contact surface features regardless of the surface waveforms. The comparative specimens with periodic waveforms designed using typical 3D printers are observed to be relatively consistent regardless of the following factors: roughness, fill pattern, peak density, kurtosis, and printing orientation. When simultaneously used with R_a, R^*_{ku} contributes to an effective evaluation and is helpful in determining the surface properties of the effective contact area, particularly for rough surfaces. From the microstructural observations of the specimen surfaces, the peeled tracks predominantly occurred in the wave peaks and the area around them, thus resulting in different bonding adhesion strengths. In addition, the peak width and depth difference in the waveforms contribute to the bonding performance. The plasma treatment of silicone rubber fabricated with 3D-printed molds is effective in enhancing the adhesion strength of soft robots.

AUTHOR INFORMATION

Corresponding Author

Yujin Jang − *Department of Mechanical Engineering, School of Engineering, Tokyo Institute of Technology, Tokyo 152-8552, Japan;* orcid.org/0000-0003-3818-2180; Email: jang.y.aa@m.titech.ac.jp

Authors

Hiroyuki Nabae − *Department of Mechanical Engineering, School of Engineering, Tokyo Institute of Technology, Tokyo 152-8552, Japan*

Koichi Suzumori − *Department of Mechanical Engineering, School of Engineering, Tokyo Institute of Technology, Tokyo 152-8552, Japan;* orcid.org/0000-0002-5735-4956

Complete contact information is available at: https://pubs.acs.org/10.1021/acsomega.2c05308

Author Contributions

Y.J. performed the investigation, methodology, software, visualization, and writing the original draft H.N. supervised the project and wrote, reviewed, and edited the manuscript. K.S. was responsible for conceptualization, funding acquisition, supervision, and writing, reviewing, and editing of the manuscript.

Notes

The authors declare no competing financial interest.

ACKNOWLEDGMENTS

This work was supported by JSPS KAKENHI under Grant 18H05470.

REFERENCES

(1) Hülse, M.; Wischmann, S.; Pasemann, F.The role of non-linearity for evolved multifunctional robot behavior. In *Lecture Notes in Computer Science*; Springer: Berlin Heidelberg, 2005; pp 108−118.

(2) Suzumori, K.; Maeda, T.; Wantabe, H.; Hisada, T.Fiberless flexible microactuator designed by finite-element method. In *IEEE/ASME Trans. Mechatron*1997; Vol. *2*, pp 281−286 DOI: 10.1109/3516.653052.

(3) Veeramuthu, L.; Cho, C. J.; Liang, F. C.; Venkatesan, M.; Kumar, G. R.; Hsu, H. Y.; Chung, R. J.; Lee, C. H.; Lee, W. Y.; Kuo, C. C. Human skin-inspired electrospun patterned robust strain-insensitive pressure sensors and wearable flexible light-emitting diodes. *ACS Appl. Mater. Interfaces* **2022**, *14*, 30160−30173.

(4) Park, Y.-L.; Chau, K.; Black, R. J.; Cutkosky, M. R. Force sensing robot fingers using embedded fiber bragg grating sensors and shape deposition manufacturing. *Proc. 2007 IEEE Int. Conf. Robot. Autom.* **2007**, 1510−1516.

(5) Santos, D.; Heyneman, B.; Kim, S.; Esparza, N.; Cutkosky, M. R. Gecko-inspired climbing behaviors on vertical and overhanging surfaces. *2008 IEEE Int. Conf. Robot. Autom.* **2008**, 1125−1131.

(6) Suzumori, K.; Koga, A.; Riyoko, H. Microfabrication of integrated FMAS using stereo lithography. *Proc. IEEE Micro Electro Mechanical Systems An Investigation of Micro Structures, Sensors, Actuators, Machines and Robotic Systems* **1994**, 136−141.

(7) Umedachi, T.; Vikas, V.; Trimmer, B. A. Highly deformable 3-D printed soft robot generating inching and crawling locomotions with variable friction legs. *2013 IEEE/RSJ Int. Conf. Intel. Robot. Syst.* **2013**, 4590−4595.

(8) Peterson, K.; Birkmeyer, P.; Dudley, R.; Fearing, R. S. A wing-assisted running robot and implications for avian flight evolution. *Bioinspiration Biomimetics* **2011**, *6*, No. 046008.

(9) Hawkes, E.; An, B.; Benbernou, N. M.; Tanaka, H.; Kim, S.; Demaine, E. D.; Rus, D.; Wood, R. J. Programmable matter by folding. *Proc. Natl. Acad. Sci. U.S.A.* **2010**, *107*, 12441−12445.

(10) Hosoda, K.; Tada, Y.; Asada, M. Anthropomorphic robotic soft fingertip with randomly distributed receptors. *Rob. Auton. Syst.* **2006**, *54*, 104−109.

https://doi.org/10.1021/acsomega.2c05308
ACS Omega 2022, 7, 45004−45013

(11) Matschuk, M.; Larsen, N. B. Injection molding of high aspect ratio sub-100 nm nanostructures. *J. Micromech. Microeng.* **2013**, *23*, No. 025003.
(12) Park, S. W.; Lee, W. I.; Moon, S. N.; Yoo, Y. -E.; Cho, Y. H. Injection molding micro patterns with high aspect ratio using a polymeric flexible stamper. *eXPRESS Polym. Lett.* **2011**, *5*, 950−958.
(13) Jang, Y.; Nabae, H.; Endo, G.; Suzumori, K. Analysis of the multi-balloon dielectric elastomer actuator for traveling wave motion. *Sens. Actuators, A* **2022**, *333*, No. 113243.
(14) Lee, H. B.; Kim, Y. W.; Yoon, J.; Lee, N. K.; Park, S. 3D customized and flexible tactile sensor using a piezoelectric nanofiber mat and sandwich-molded elastomer sheets. *Smart Mater. Struct.* **2017**, *26*, No. 045032.
(15) Georgopoulou, A.; Michel, S.; Vanderborght, B.; Clemens, F. Piezoresistive sensor fiber composites based on silicone elastomers for the monitoring of the position of a robot arm. *Sens. Actuators, A* **2021**, *318*, No. 112433.
(16) Hwang, Y.; Paydar, O. H.; Candler, R. N. Pneumatic microfinger with balloon fins for linear motion using 3D printed molds. *Sens. Actuators, A* **2015**, *234*, 65−71.
(17) Zhou, J.; Chen, S.; Wang, Z.A soft-robotic gripper with enhanced object adaptation and grasping reliability. *IEEE Robot. Autom. Lett.*, 2017, *2*, 2287−2293.
(18) Zhang, N.; Liu, J.; Zhang, H.; Kent, N. J.; Diamond, D.; D Gilchrist, M. 3D printing of metallic microstructured mould using selective laser melting for injection moulding of plastic microfluidic devices. *Micromachines* **2019**, *10*, 595.
(19) Bauer, S.; Bauer-Gogonea, S.; Grza, I.; Kaltenbrunner, M.; Keplinger, C.; Schwödiauer, R. 25th anniversary article: A soft future: from robots and sensor skin to energy harvesters. *Adv. Mater.* **2014**, *26*, 149−161.
(20) Majidi, C. Soft robotics: A perspective—current trends and prospects for the future. *Soft Rob.* **2014**, *1*, 5−11.
(21) Dickey, M. D. Emerging applications of liquid metals featuring surface oxides. *ACS Appl. Mater. Interfaces* **2014**, *6*, 18369−18379.
(22) Marchese, A. D.; Katzschmann, R. K.; Rus, D. A recipe for soft fluidic elastomer robots. *Soft Rob.* **2015**, *2*, 7−25.
(23) Onal, C. D.; Rus, D. Autonomous undulatory serpentine locomotion utilizing body dynamics of a fluidic soft robot. *Bioinspiration Biomimetics* **2013**, *8*, No. 026003.
(24) Calisti, M.; Giorelli, M.; Levy, G.; Mazzolai, B.; Hochner, B.; Laschi, C.; Dario, P. An octopus-bioinspired solution to movement and manipulation for soft robots. *Bioinspiration Biomimetics* **2011**, *6*, No. 036002.
(25) Miyakawa, N.; Minamisawa, S.; Takikawa, H.; Sakakibara, T.Physical−chemical hybrid deposition of DLC film on rubber by T-shape filtered-arc-deposition. In *Vacuum*; Elsevier, 2004; Vol. *73*, pp 611−617.
(26) Wakimoto, S.; Ogura, K.; Suzumori, K.; Nishioka, Y. Miniature soft hand with curling rubber pneumatic actuators. *2009 IEEE Int. Conf. Robot. Autom.* **2009**, 556−561.
(27) Zhou, Y.; Chen, M.; Ban, Q.; Zhang, Z.; Shuang, S.; Koynov, K.; Butt, H. J.; Kong, J.; Wu, S. Light-switchable polymer adhesive based on photoinduced reversible solid-to-liquid transitions. *ACS Macro Lett.* **2019**, *8*, 968−972.
(28) Yoshida, S.; Okoshi, M.; Inoue, N. Femtosecond-pulsed laser deposition of diamond-like carbon films onto silicone rubber. *J. Phys.: Conf. Ser.* **2007**, *59*, 368−371.
(29) Yamamoto, T. Solid-state bonding of silicone elastomer to glass by vacuum oxygen plasma, atmospheric plasma, and vacuum ultraviolet light treatment. *Surf. Interface Anal.* **2013**, *45*, 817−822.
(30) Gaboury, S. R.; Urban, M. W. Microwave plasma reactions of solid monomers with silicone elastomer surfaces: a spectroscopic study. *Langmuir* **1993**, *9*, 3225−3233.
(31) Lai, J. Y.; Lin, Y. Y.; Denq, Y. L.; Shyu, S. S.; Chen, J. K. Surface modification of silicone rubber by gas plasma treatment. *J. Adhes. Sci. Technol.* **1996**, *10*, 231−242.
(32) Luzanin, O.; Movrin, D.; Plancak, M. Experimental investigation of extrusion speed and temperature effects on arithmetic mean surface roughness in FDM-built specimens. *J. Technol. Plast.* **2013**, *38*, 179−190.
(33) Ahn, D.; Kweon, J.; Kwon, S.; Spog, J.; Lee, S. Representation of surface roughness in fused deposition modeling. *J. Mater. Process Technol.* **2009**, *209*, 5593−5600.
(34) Campbell, R. I.; Martorelli, M.; Lee, H. S. Surface roughness visualisation for rapid prototyping models. *Comput.-Aided Des.* **2002**, *34*, 717−725.
(35) Vasudevarao, B.; Natarajan, D. P.; Henderson, M.; Razdan, A. In *Sensitivity of RP Surface Finish to Process Parameter Variation*, International Solid Freeform Fabrication Symposium, 2000; pp 251−258.
(36) Pérez, C. J. L. Analysis of the surface roughness and dimensional accuracy capability of fused deposition modelling processes. *Int. J. Prod. Res.* **2002**, *40*, 2865−2881.
(37) Gad, M. M.; Fouda, S. M.; Abualsaud, R.; Alshahrani, F. A.; Al-Thobity, A. M.; Khan, S. Q.; Akhtar, S.; Ateeq, I. S.; Helal, M. A.; Al-Harbi, F. A. Strength and surface properties of a 3D-printed denture base polymer. *J. Prosthodont.* **2022**, *31*, 412−418.
(38) Gadelmawla, E. S.; Koura, M. M.; Maksoud, T. M. A.; Elewa, I. M.; Soliman, H. H. Roughness parameters. *J. Mater. Process. Technol.* **2002**, *123*, 133−145.
(39) Wang, W.-z.; Chen, H.; Hu, Y.; Wang, H. Effect of surface roughness parameters on mixed lubrication characteristics. *Tribol. Int.* **2006**, *39*, 522−527.
(40) Jeng, Y. R. Impact of plateaued surfaces on tribological performance. *Tribol. Trans.* **1996**, *39*, 354−361.
(41) Michalski, J.; Pawlus, P. Description of honed cylinders surface topography. *Int. J. Mach. Tools Manuf.* **1994**, *34*, 199−210.
(42) Tayebi, N.; Polycarpou, A. A. Modeling the effect of skewness and kurtosis on the static friction coefficient of rough surfaces. *Tribol. Int.* **2004**, *37*, 491−505.
(43) Kotwal, C. A.; Bhushan, B. Contact analysis of non-Gaussian surfaces for minimum static and kinetic friction and wear. *Tribol. Trans.* **1996**, *39*, 890−898.

https://doi.org/10.1021/acsomega.2c05308
ACS Omega 2022, 7, 45004−45013